PROCEEDINGS OF SCIENCE

The curvature of the crossover line in the (T, μ)-phase diagram of QCD

Rene Bellwied

Department of Physics, University of Houston, Houston, TX 77204, USA

Szabolcs Borsanyi

Department of Physics, Wuppertal University, Gaussstr. 20, D-42119 Wuppertal, Germany

Zoltan Fodor
Department of Physics, Wuppertal University, Gaussstr. 20, D-42119 Wuppertal, Germany
Inst. for Theoretical Physics, Eötvös University
Jülich Supercomputing Centre, Forschungszentrum Jülich, D-52425 Jülich, Germany

Jana Günther*
Department of Physics, Wuppertal University, Gaussstr. 20, D-42119 Wuppertal, Germany
E-mail: Jana.Guenther@t-online.de

Sandor D. Katz
Inst. for Theoretical Physics, Eötvös University
MTA-ELTE "Lendület" Lattice Gauge Theory Research Group, Budapest, Hungary

Claudia Ratti

Department of Physics, University of Houston, Houston, TX 77204, USA

Kalman K. Szabo
Department of Physics, Wuppertal University, Gaussstr. 20, D-42119 Wuppertal, Germany
Jülich Supercomputing Centre, Forschungszentrum Jülich, D-52425 Jülich, Germany

An efficient way to study the QCD phase diagram at small finite density is to extrapolate thermodynamical observables from imaginary chemical potential. The phase diagram features a crossover line starting from the transition temperature already determined at zero chemical potential. In this talk we focus on the curvature of this line at mu = 0. We present the extrapolation of the crossover temperature based on three observables at several lattice spacings. The simulations were performed at zero and at moderate values of the imaginary chemical potential, always in the strangeness neutral point. We used the Symanzik-improved gauge action with four times stout smeared staggered fermions.

The 33rd International Symposium on Lattice Field Theory
14 -18 July 2015
Kobe International Conference Center, Kobe, Japan

*Speaker.

PoS(LATTICE 2015)142

1. Introduction

Since we cannot determine the crossover temperature at real finite μ_B with direct lattice simulations, we determine the curvature at $\mu_B = 0$ and extrapolate the crossover temperature to finite μ_B. A parametrisation that respects respects symmetry under charge conjugation at $\mu_B = 0$ is

$$\frac{T_c(\mu_B)}{T_c(0)} = 1 - \kappa \left(\frac{\mu_B}{T_c(\mu_B)} \right)^2 + \mathcal{O}(\mu_B^4). \tag{1.1}$$

There are two main methods to determine κ: The Taylor expansion method as in [1, 2] or the method of analytic continuation [3, 4, 5, 6]. In this work we will present continuum extrapolated results from $40^3 \times 10$, $48^3 \times 12$ and $64^3 \times 16$ lattices with the method of analytic continuation as well as a comparison to the Taylor expansion on $40^3 \times 10$ lattices.

In this proceedings we can only give a brief introduction with a summary of the most resent results. For a more detailed overview please see [7] and references therein.

2. Simulation details

We use a tree-level Symanzik improved gauge action, with four times stout smeared ($\rho = 0.125$) staggered fermions. We simulate $2+1+1$ dynamical quarks where the light flavors are tuned in a way to reproduce the physical pion and kaon mass and we set $\frac{m_c}{m_s} = 11.85$ [8]. For the zero temperature runs we use large volumes which full fill $Lm_\pi > 4$. The scale is determined by using f_π ans w_0 as two alternative methods for scale setting. More Details can be found in [7].

The maximal useful value of m_B is $m_B = i\pi T$ because of the Roberge-Weiss transition [9]. We simulate at six different values of m_B given as: $\mu_B^{(j)} = iT\frac{j\pi}{8}$ for $j \in \{0,1,2,3,4,5,6\}$. The simulations as $\mu_B = 0$ are used to obtain a "baseline" for the shift in the transition at imaginary μ_B and to do a Taylor expansion in one observable to compare it with the method of analytic continuation. The data at $j = 1,2,6$ is not used for the calculation of κ. At $j = 1,2$ it is only used to tune the simulations to the strangeness neutral point (see section 3) and at $j = 6$ it is used to estimate the uncertainties in 3.

We performed simulations on $32^3 \times 8$, $40^3 \times 10$, $48^3 \times 12$ and $64^3 \times 16$ lattices, at sixteen temperatures in the temperature range 135...210 MeV. We have generated between 10000-15000 Hybrid Monte Carlo updates, analyzing every 5th of them (every 10th for $N_t = 16$). The configurations have been evaluated for up to fourth order generalized quark number susceptibilities [7] and for the chiral condensate and susceptibility. For $\mu_B = 0$ we have 5 ... 10 times more statistics. This ensures a solid guidance to the fitting procedure.

3. Strangeness neutrality

The interpretation of μ_B varies between different references. In [10] simulations are performed at $\mu_u = \mu_d = \mu_s = \frac{\mu_B}{3}$. On the other hand [3] looks at two different possibilities: $\mu_u = \mu_d = \mu_s = \frac{\mu_B}{3}$ as well as $\mu_u = \mu_d = \frac{\mu_B}{3}$ and $\mu_s = 0$. In this work we want to choose our simulations by the situation realised in experiment. Since the nuclei used for heavy ion collisions do not contain strange quarks

we want to simulate with $\langle n_S \rangle = 0$ for each μ_B. To avoid heavy tuning we will describe a procedure we used to solve the equation

$$\langle n_S \rangle = 0 \Leftrightarrow \frac{\partial \log Z}{\partial \mu_S} = 0. \tag{3.1}$$

Our aim is to determine μ_S in a way that $\langle n_S \rangle = 0$ for a given μ_B. In the following the index of χ will imply the derivative of the partition sum with respect to a chemical potential. For example

$$\chi_{BQS} = -\frac{1}{T^4} \frac{\partial^3}{\partial(\mu_B/T)\partial(\mu_Q/T)\partial(\mu_S/T)} \frac{T}{V} \log Z.$$

Assuming we know the value for $\mu_S(\mu_B)$ so that $\langle n_s \rangle = 0$ for $\mu_S(\mu_B^0)$ and $\mu_S(\mu_B^0 - \Delta\mu_B)$ as well as the derivative $\frac{\mathrm{d}\mu_S}{\mathrm{d}\mu_B}(\mu_B^0)$ with infinite precession. We can then calculate the correct value for μ_S at $\mu_B^0 + \Delta\mu_B$ by a simple Runge-Kutta step:

$$\mu_S(\mu_B^0 + \Delta\mu_B) = \mu_S(\mu_B^0 - \Delta\mu_B) + 2\Delta\mu_B \frac{\mathrm{d}\mu_S}{\mathrm{d}\mu_B}(\mu_B^0).$$

In the simulations with μ_B^0 and $\mu_B^0 - \Delta\mu_B$, μ_S might not precisely tuned and we will never reach infinite precession. Therefore we will extrapolate to a corrected value, so that errors made in previous steps will not accumulate. We assume that the correct value of μ_S is $\tilde{\mu}_S = \mu_S' + \Delta\mu_S'$. By a Taylor expansion we get:

$$\langle n_S \rangle = \frac{\partial \log Z}{\partial \tilde{\mu}_S} = \frac{\partial \log Z}{\partial \mu_S'} + \frac{\partial^2 \log Z}{\partial \mu_S'^2} \Delta\mu_S' = 0$$

This yields $\Delta\mu_S' = -\frac{\chi_{SB}}{\chi_{SS}}$. This result we can now use to correct our previous values for $\mu_S(\mu_B^0)$ and $\mu_S(\mu_B^0 - \Delta\mu_B)$. The derivative $\frac{\mathrm{d}\mu_S}{\mathrm{d}\mu_B}(\mu_B^0)$ can be corrected in a similar way.

4. Analysis

A more detailed description of our analysis can be found in [7]. We analyse three different observables. Further information concerning definition and renormalization can be found in [11].

The first observable is the chiral susceptibility, defined and renormelized by substracting the zero temperature data as:

$$\chi_{\bar{\psi}\psi} = \frac{T}{V} \frac{\partial^2 \ln Z}{\partial (m_q)^2}, \quad \chi^r_{\bar{\psi}\psi} = \left(\chi_{\bar{\psi}\psi}(T,\beta) - \chi_{\bar{\psi}\psi}(0,\beta)\right) \frac{m_l^2}{m_\pi^4}. \tag{4.1}$$

The chiral susceptibility has the form of a peak that is shifted to higher temperatures with increasing chemical potential. The shape of the peak varies only sightly with the chemical potential and this variation can be described by a change of the hight and the width of the peak. This allows us to fit the peaks for one lattice size but different chemical potentials simultaneously. This allows us to determine the shape of the peak mostly by the data for $\mu_B = 0$ which has the highest statistics (see section 2). We are using two different ansatzes:

$$\chi^r_{\bar{\psi}\psi}(\mu,T) = \begin{cases} C + A^2(\mu)\left(1 + W^2(\mu)(T - T_c(\mu))^2\right)^{\alpha/2} & \text{for } T \le T_c \\ C + A^2(\mu)\left(1 + b^2 W^2(\mu)(T - T_c(\mu))^2\right)^{\alpha/2} & \text{for } T > T_c \end{cases} \tag{4.2}$$

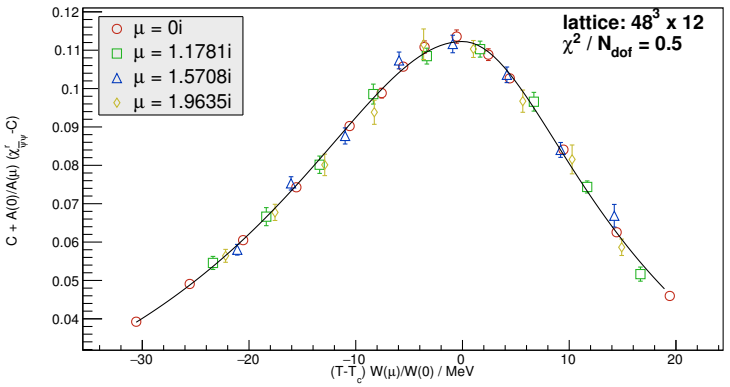

Figure 1: The chiral susceptibility for an $48^3 \times 12$ lattice after the rescaling of the date for finite chemical potential.

and

$$\chi^r_{\bar{\psi}\psi}(\mu,T) = C + \frac{A(\mu)}{1+W^2(\mu)(T-T_c(\mu))^2 + a_3 W^3(\mu)(T-T_c(\mu))^3}. \tag{4.3}$$

For the zero temperature data (that is needed for the renormalization) we use to different function for the interpolation:

$$\chi_{\bar{\psi}\psi}(0,\beta) = \sum_{k=0}^{6} A_k \beta^k \quad \text{and} \quad \chi_{\bar{\psi}\psi}(0,\beta) = \sum_{k=-2}^{2} A_k \beta^k. \tag{4.4}$$

We choose the fit windows by selecting three different values for $\chi^r_{\bar{\psi}\psi}$ and neglecting all data points below that value. If we rescale the data for finite chemical potential appropriately they all lie on top of the curve for $\mu_B = 0$ as shown in figure 1 To account for the correlation of the different data sets introduced by the subtraction of the zero temperature data we combine the fits for different lattice sizes and for the zero temperature data in one large fit to avoid a large correlation matrix. All fit parameters in equation 4.2 and 4.3 can be different for each lattice size. To determine κ we use again two different methods. First we determine κ by doing a linear fit of $\frac{T_c((\mu_B/T_c)^2)}{T_c(0)}$ vs. μ_B/T_c and extrapolate κ to the continuum. As a second method we do a combined μ_B and continuum fit. Since the χ^2 value for a continuum fit with all four lattice spacings was large we included only the lattices $40^3 \times 10$, $48^3 \times 12$ and $64^3 \times 16$ in our final analysis. This leads to good values for χ^2.

The other two observables are the chiral condensate

$$\langle\bar{\psi}\psi\rangle = \frac{T}{V}\frac{\partial \ln Z}{\partial m_q}, \quad \langle\bar{\psi}\psi\rangle^r = -\left(\langle\bar{\psi}\psi\rangle(T,\beta) - \langle\bar{\psi}\psi\rangle(0,\beta)\right)\frac{m_l}{m_\pi^4} \tag{4.5}$$

and the strange susceptibility χ^E_{SS}. Both have a step like form and we fit them with the ansatzes

$$\langle\bar{\psi}\psi\rangle^r(\mu,T) = A(\mu)\left(1 + B\tanh\left[C\left(T - T_c(\mu)\right)\right] + D\left(T - T_c(\mu)\right)\right) \tag{4.6}$$

and

$$\langle\bar{\psi}\psi\rangle^r(\mu,T) = A(\mu)\left(1 + B\arctan\left[C\left(T - T_c(\mu)\right)\right] + D\left(T - T_c(\mu)\right)\right). \tag{4.7}$$

The strange susceptibility has the advantage that it needs no renormalization. For the renormalization of the chiral condensate we fit the zero temperature data with polynomials of order six or seven. The rest of the analysis works analogously to the analysis of the chiral susceptibility.

To estimate the statistical error we combine the different analysis methods in a histogram and use the central 68% of the histogram as an estimate of the systematic error. The statistical error is obtained from 1000 bootstrap samples. We combine the two errors by quadrature in final combined error. The resulting histograms can be seen on the left side of figure 2.

The histograms of the three quantities can be joined into a single one leading to our combined result based on our three observables with strangeness neutrality:

$$\kappa = 0.0149 \pm 0.0021. \tag{4.8}$$

Our simulations were done at $\langle n_S \rangle = 0$ and $0.5\langle B \rangle = \langle Q \rangle$. To compare our results with experiments it would be better to simulate at $\langle n_S \rangle = 0$ and $0.4\langle B \rangle = \langle Q \rangle$. Therefore we extrapolated the strange susceptibility to this point (χ_{SS}). As it can be seen on the left side of figure 2 the effect is negligible within the errors.

In addition to using the method of analytic continuation we also used our $\mu_B = 0$ data to perform an analysis by doing a Taylor expansion. More details on this analysis can be found in [7]. The results can be found on the right side of figure 2.

Finally we use our results to extrapolate to finite real μ_B. To estimate the systematics and the validity range of the extrapolation we fit $\frac{T_c((\mu_B/T_c)^2)}{T_c(0)}$ with the functions $1+ax$, $1+ax+bx^2$, $\frac{1+ax}{1+bx}$ and $\frac{1}{1+ax+bx^2}$. In these fits we include the data for $j = 6$ to have a better control over the second order influences. The results for $\langle \bar{\psi}\psi \rangle$ is shown in figure 3.

5. Conclusion

The present result indicates a stronger curvature than the one presented in Ref. [1]. There are, however a couple differences between the definitions/ approaches of the curvature of the present analysis and Ref. [1]. Note that the transition is a smooth cross-over, thus different definitions obviously lead to different results.

In Ref. [1] we used a vanishing strangeness chemical potential. In the present analysis we use instead vanishing strange density. The reason for this change is to be as close to the experimental situation as possible. In heavy ion collisions the net strangeness is zero.

It is emphasized in the discussion of Figure 5 of [1] that only statistical uncertainties were provided. The present analysis estimates systematic uncertainties coming from various aspects of the analysis as discussed earlier. These are comparable to or in some cases even larger than the statistical uncertainties. A similar assumption on the systematics of Ref. [1] would make the tension between the results much weaker.

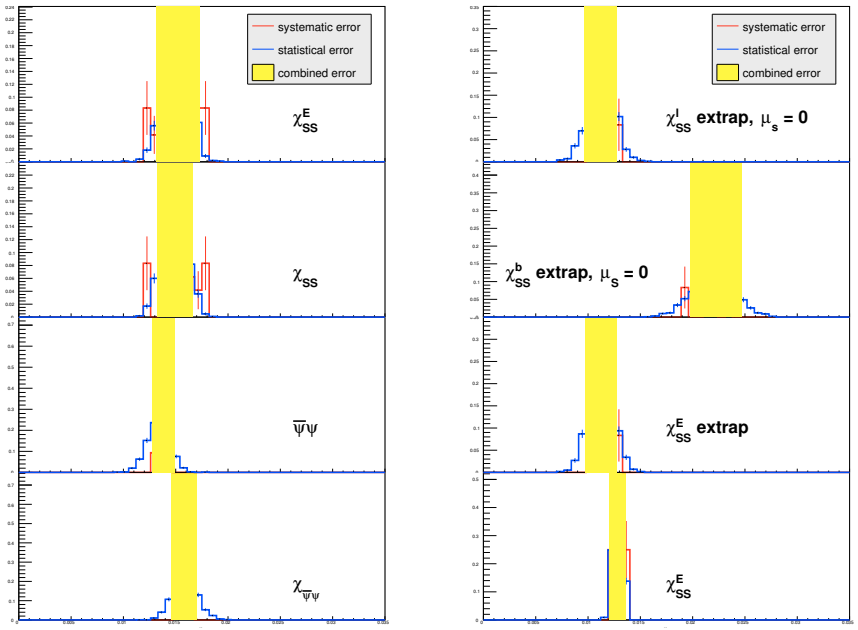

Figure 2: Left: The continuum extrapolated results from the analytic continuation for the curvatrue κ at $\mu_B = 0$. Here χ_{SS} is at $Z = 0.5A$ and χ^E_{SS} is extrapolated to $Z = 0.4A$. Both are extrapolated to the strangeness neutral point. Right: The results obtained by Taylor expansion for $\mu_s = 0$ (χ^l_{SS}), $\mu_S = 0$ (χ^b_{SS}) and at the strangness neutral point (χ^E_{SS}) as well as χ^E_{SS} obtained from analytic continuation on a $40^3 \times 10$ lattice.

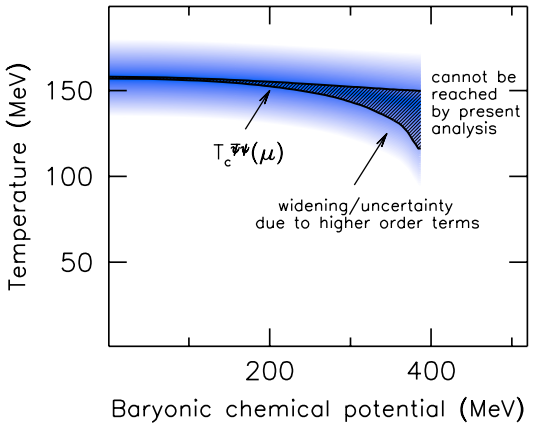

Figure 3: The extrapolation to finite chemical potential.

6. Acknowledgements

The authors thank G. Endrodi for his valuable comments and suggestions. This project was funded by the DFG grant SFB/TR55. S. D. Katz is funded by the "Lendület" program of the Hungarian Academy of Sciences ((LP2012-44/2012). The work of R. Bellwied is supported through DOE grant DEFG02-07ER41521. An award of computer time was provided by the INCITE program. The work of C. R. is supported by the National Science Foundation through grant number NSF PHY-1513864 This research used resources of the Argonne Leadership Computing Facility, which is a DOE Office of Science User Facility supported under Contract DE- AC02-06CH11357. This research also used resources of the PRACE Research Infrastructure resource JUQUEEN at FZ-Jülich, Germany; JUQUEEN as large scale project of the Gauss Centre for Supercomputing (GCS); the QPACE machine supported by the Deutsche Forschungsgesellschaft through the research program SFB TR55; and the GPU cluster at the Wuppertal University.

References

[1] G. Endrodi, Z. Fodor, S. D. Katz, und K. K. Szabo, *The QCD phase diagram at nonzero quark density*, *JHEP* **04** (2011) 001, [arXiv:1102.1356].

[2] O. Kaczmarek, F. Karsch, E. Laermann, C. Miao, S. Mukherjee, P. Petreczky, C. Schmidt, W. Soeldner, und W. Unger, *Phase boundary for the chiral transition in (2+1) -flavor QCD at small values of the chemical potential*, *Phys. Rev.* **D83** (2011) 014504, [arXiv:1011.3130].

[3] C. Bonati, M. D'Elia, M. Mariti, M. Mesiti, F. Negro, und F. Sanfilippo, *Curvature of the chiral pseudocritical line in QCD*, *Phys. Rev.* **D90** (2014), no. 11 114025, [arXiv:1410.5758].

[4] C. Bonati, M. D'Elia, M. Mariti, M. Mesiti, F. Negro, und F. Sanfilippo, *Curvature of the chiral pseudo-critical line in QCD: continuum extrapolated results*, arXiv:1507.0357.

[5] P. Cea, L. Cosmai, und A. Papa, *Critical line of 2+1 flavor QCD*, *Phys. Rev.* **D89** (2014), no. 7 074512, [arXiv:1403.0821].

[6] M. Mesiti, C. Bonati, M. D'elia, M. Mariti, F. Negro, und F. Sanfilippo, *The curvature of the QCD critical line from analytic continuation*, *PoS* **LATTICE2014** (2015) 174.

[7] R. Bellwied, S. Borsanyi, Z. Fodor, J. Günther, S. D. Katz, C. Ratti, und K. K. Szabo, *The QCD phase diagram from analytic continuation*, arXiv:1507.0751.

[8] C. McNeile, C. T. H. Davies, E. Follana, K. Hornbostel, und G. P. Lepage, *High-Precision c and b Masses, and QCD Coupling from Current-Current Correlators in Lattice and Continuum QCD*, *Phys. Rev.* **D82** (2010) 034512, [arXiv:1004.4285].

[9] A. Roberge und N. Weiss, *Gauge Theories With Imaginary Chemical Potential and the Phases of QCD*, *Nucl. Phys.* **B275** (1986) 734.

[10] L. Cosmai, P. Cea, und A. Papa, *Curvature of the QCD critical line with 2+1 HISQ fermions*, *PoS* **LATTICE2014** (2014) 171, [arXiv:1410.2471].

[11] **Wuppertal-Budapest** Kollaboration, S. Borsanyi, Z. Fodor, C. Hoelbling, S. D. Katz, S. Krieg, C. Ratti, und K. K. Szabo, *Is there still any T_c mystery in lattice QCD? Results with physical masses in the continuum limit III*, *JHEP* **09** (2010) 073, [arXiv:1005.3508].